ISSN 2070-2051, Protection of Metals and Physical Chemistry of Surfaces, 2021, Vol. 57, No. 3, pp. 550–558. © Pleiades Publishing, Ltd., 2021.
Russian Text © The Author(s), 2021, published in Fizikokhimiya Poverkhnosti i Zashchita Materialov, 2021, Vol. 57, No. 3, pp. 312–321.

NEW SUBSTANCES, MATERIALS, AND COATINGS

Corrosion Behavior of Modified Anodic Oxide Coatings on AD31 Aluminium Alloy

M. A. Osipenko[a], *, D. S. Kharitonov[b], **, I. V. Makarova[c], V. I. Romanovsky[d], and I. I. Kurilo[a]

[a] *Belarusian State Technological University, Minsk, 220006 Belarus*
[b] *Jerzy Haber Institute of Catalysis and Surface Chemistry of Polish Academy of Sciences, Krakow, 30-239 Poland*
[c] *Lappeenranta University of Technology, Lappeenranta, Finland*
[d] *Institute of General and Inorganic Chemistry of National Academy of Sciences of Belarus, Minsk, 220072 Belarus*
**e-mail: marikaosipenko@gmail.com*
***e-mail: Dmitry.Kharitonov@ikifp.edu.pl*

Received August 24, 2020; revised December 10, 2020; accepted January 12, 2021

Abstract—The dependences of the protective properties of the anodic oxide coatings on the AD31 aluminum alloy surface modified with nitrates of magnesium, potassium, and some 3*d*-elements on the composition of sealing solutions and parameters of finishing treatment were established by scanning electron microscopy, potentiodynamic polarization, electrochemical impedance spectroscopy, and salt spray chamber tests. A mechanism of the formation of modified anodic oxide coatings during sealing and subsequent thermal treating was proposed.

Keywords: AD31 alloy, anodic treatment, sealing, metal nitrates, thermal treatment
DOI: 10.1134/S2070205121030175

INTRODUCTION

In recent decades, the development of lightweight, durable metal materials displaying high mechanical and anticorrosion properties has attracted considerable attention. Aluminum alloys have a considerable advantage in these indicators over other widely used industrial metals—for example, magnesium alloys.

A naturally occurring anodic oxide layer formed on the surface of aluminum alloys in contact with moisture and air provides sufficient corrosion protection in many moderately aggressive media [1]. Nevertheless, in many cases of industrial applications, aluminum alloys require advanced corrosion prevention. For this purpose, electrochemical formation of anodic oxide coating (AOC) with a required structure, thickness, and hardness is used.

The AOC thickness and structure are determined by the parameters of anodization: electrolyte type, voltage or current density, temperature, agitation, etc. [2]. The most common anodization is carried out in acid solutions, producing a coating composed of internal nonporous and external porous layers [3]. An increase in the AOC thickness occurs with the retention of porosity, and subsequent sealing (compaction, finish treatment) is required for improving corrosion resistance [4].

AOC sealing is traditionally performed in hot distilled water or solutions of chromium(VI) compounds. However, it is promising to employ electrolytes containing less hazardous compounds [5]. A set of new methods and electrolytes have been developed for the AOC sealing. High-temperature sealing in a solution of nickel fluoride is most commonly used in industry [6]. Chahboun et al. [7] proposed the chemical sealing of the porous oxide layer by a mixture of Zr(IV) and Cr(III) salts, which enabled them to increase the corrosion resistance of the surface by about 300 times compared to the standard hydrothermal sealing. Yu et al. [8] provided evidence of the efficiency of cerous nitrate for the AOC sealing. Potassium permanganate was also found to be efficient for the AOC sealing [9].

Thus, the search for environmentally friendly and economically viable sealing solutions is of practical interest for fabricating anodic oxide coatings on aluminum alloys.

The purpose of the work is to study the effect of the composition of sealing electrolytes and parameters of finishing treatment on the corrosion behavior of anodic oxide coatings on the AD31 aluminum alloy modified with calcium, magnesium, and some 3*d* group metals.

EXPERIMENTAL

AD31 (AA6063) aluminum alloy was used as an object of the study. The anodization was carried out using an Elatek B5-80 current source for 40 min at room temperature (≈22°C) and a current density of

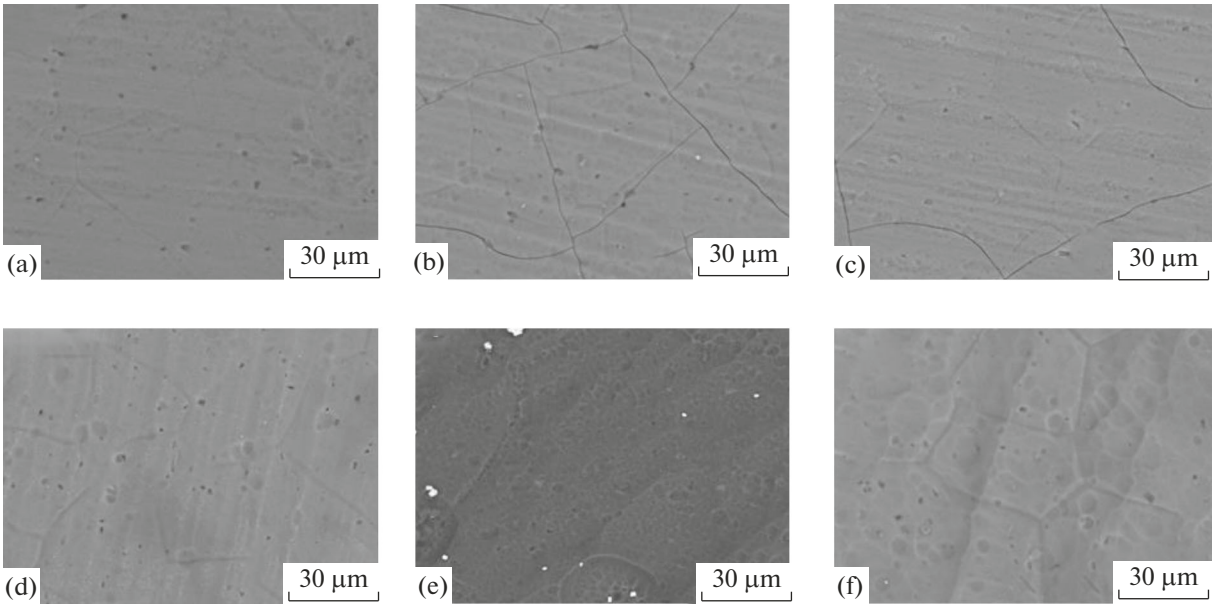

Fig. 1. Micrographs of AOC samples sealed in 0.2 M solutions: (a) $Mg(NO_3)_2$, (b) $Ca(NO_3)_2$, (c) $Zn(NO_3)_2$, (c) $Ni(NO_3)_2$, (e) $Co(NO_3)_2$ and (f) $Cu(NO_3)_2$.

1 A/dm^2 in sulfuric acid electrolyte containing 2.0 mol/dm^3 H_2SO_4; lead was used as the cathode material. Before the process, the samples were prepared following the State standard *GOST* 9.402–2004. The subsequent AOC sealing was performed using the method of horizontal immersion of oxidized samples into the working solutions, containing 0.2 mol/dm^3 of one of the salts $Mg(NO_3)_2$, $Ca(NO_3)_2$, $Zn(NO_3)_2$, $Ni(NO_3)_2$, $Co(NO_3)_2$ or $Cu(NO_3)_2$. The temperature of the solutions was 100 ± 1°C, and the sealing time was 20 min. After the sealing, the samples were washed with distilled water and dried using a hot-air gun.

The sealed samples were treated by thermal finish polishing finishing treatment in a muffle furnace at the temperature of 300 ± 1°C, and the annealing time was 30 min.

The elemental composition and morphology of the coatings were studied by scanning electron microscopy (SEM) and energy-dispersive X-ray microanalysis (EDX) using a JEOL JSM–5610 LV microscope equipped with a chemical X-ray microanalysis EDX JED-2201 system.

The corrosion resistance of the prepared coatings exposed to 0.5 M sodium chloride solution was estimated using a PGSTAT 302N potentiostat/galvanostat (Methrom Autolab) equipped with a FRA32M impedance analyzer module. A saturated silver/silver-chloride electrode was used as a reference electrode, and a platinum mesh was used as a counter electrode. The potentiodynamic polarization curves were recorded within the range of potentials from –300 to +300 mV versus the open-circuit potential (OCP) at a scan rate of 1 mV/s.

The impedance spectra were recorded over the frequency range of 10^5–10^{-2} Hz using the current perturbation amplitude of 10 mV. ZView 3.2 and Nova 2.1 software were employed to analyze spectra, select the equivalent circuit, and calculate the parameters of their elements.

The prepared coatings were tested in a S120is (ASCOTT) salt spray chamber according to ASTM B117–16 standard practice. One side of the sample was subjected to the tests, and the reverse side was insulated with KO-85 silicone varnish. The samples were exposed to a 5% NaCl solution for 510 h at the temperature of 35 ± 2°C. When analyzing the surface state, the samples were periodically removed from the chamber, washed with distilled water, dried, and photographed with a Nikon D60 digital camera.

RESULTS AND DISCUSSION

As a result of the anodization in the solution of sulfuric acid, the gray anodic oxide coating with a thickness of about 20 μm was formed on the surface of the AD31 alloy. Figures 1 and 2 depict the SEM images of the AOC surface sealed in the $Mg(NO_3)_2$, $Ca(NO_3)_2$, $Zn(NO_3)_2$, $Ni(NO_3)_2$, $Co(NO_3)_2$ and $Cu(NO_3)_2$ solutions with and without subsequent thermal treatment, respectively.

As is evident from the microphotographs, the AOC sealing in the solutions of the studied nitrates results in the formation of the coatings with a large number of microinclusions (Figs. 1a–1e). All coatings demonstrate a heterogeneous structure. Moreover, cavities and cracks are found on the surface of some samples.

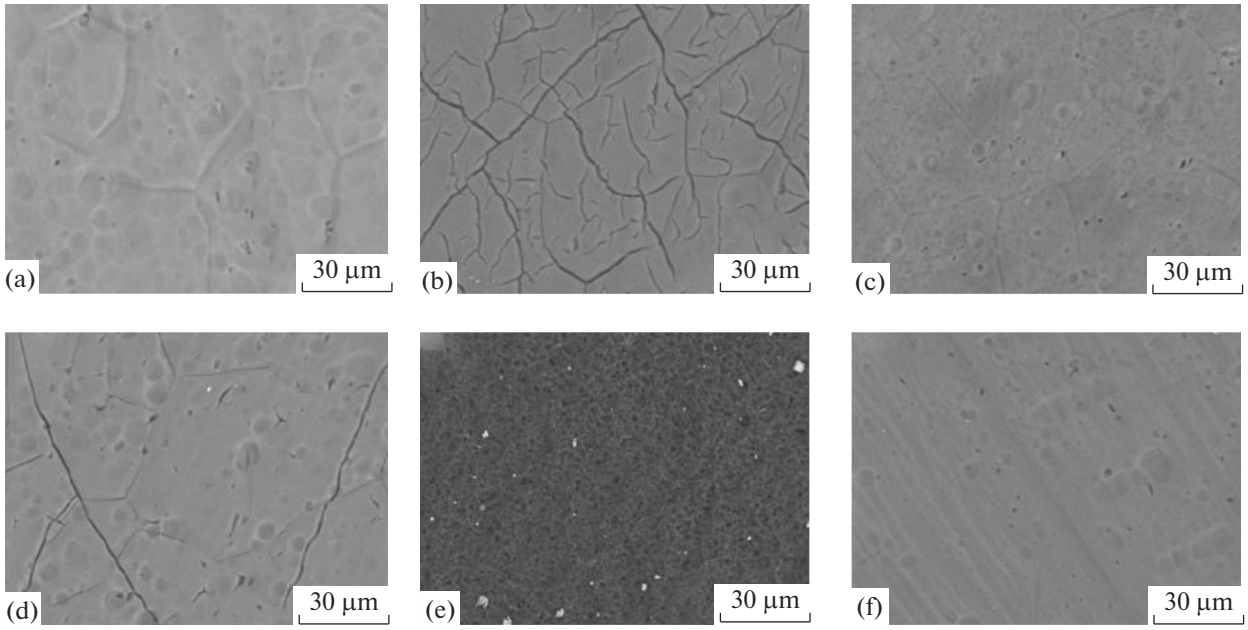

Fig. 2. SEM images of AOC samples sealed in 0.2 M solutions: (a) $Mg(NO_3)_2$, (b) $Ca(NO_3)_2$, (c) $Zn(NO_3)_2$, (c) $Ni(NO_3)_2$, (e) $Co(NO_3)_2$ and (f) $Cu(NO_3)_2$ after annealing for 30 min at a temperature of 300°C.

The AD31 alloy contains additives in the form of anodic and cathodic intermetallic particles [9–12]. Selective dissolution of these particles during anodizing may significantly affect the AOC structure. A difference between the chemical compositions of the aluminum matrix and intermetallic particles leads to the changes in pore morphology, defects and cracks generated by excess internal stresses in the formed oxide layer [12–14]. It should be noted that preliminary washing of the AOC layer results in the fact that at the early stage of sealing, the temperature in the depth of the pores is lower than at the surface, which can contribute to the initiation of mechanical stresses and cracking of the AOC samples [14–16].

The thermal treatment of the sealed AOCs can lead to the crystallization of the amorphous oxide layer and modifying agent, having a significant impact on the microstructure and protective properties of the formed coatings. The microphotographs of the sample surface after annealing at the temperature of 300°C for 30 min demonstrate a noticeable escalation of the total heterogeneity of the coating surface, local defects, and an increase in the number of microcracks (see Fig. 2). This can be attributed to the increased brittleness of the coating and its cracking during annealing [16, 17].

The EDX elemental analysis of the modified AOC sample (Table 1) revealed that the formed AOCs were predominantly composed of aluminum, oxygen, and sulfur. The significant sulfur content in the coating structure is determined by using the sulfur acid as the anodizing electrolyte. The content of the primary component of the modifying solution (metal) in the AOC structure was found in the range from 0.30 to 13.4 wt %, depending on the composition of the sealing electrolyte. The thermal treatment at 300°C results in an increase in the content of the modifying agent in the coating structure by 0.30–0.50 wt %.

The AOC corrosion resistance was examined by electrochemical methods. Figure 3 shows the potentiodynamic polarization curves of the prepared AOC samples.

The sealing in nitrate solutions significantly affects the OCP values of the AOC samples in 0.5 M NaCl solution. The OCP of all the AOC samples other than those sealed in the $Mg(NO_3)_2$ and $Cu(NO_3)_2$ solutions shifted towards the electropositive region compared to the unsealed sample. This fact is indicative of the effective incorporation of modifying components into the AOC structure.

When the sealing is carried out in the $Cu(NO_3)_2$ solution, the OCP value almost does not change, whereas the sealing is in the $Mg(NO_3)_2$ solution results in the shift of the OCP towards the electronegative region by 150 ± 5 mV. For all the AOC samples other than those sealed in the $Cu(NO_3)_2$ solution, a decrease in the corrosion current density is observed, and, as a consequence, their protective properties are enhanced compared to the unsealed sample (Table 2). These behaviors were interpreted as a result of the filling of pores, which are formed in the AOCs during the process of anodizing, with the modifying solution. The sealing provides the pore blocking and hermetic encapsulation of the oxide layer of the sample surface. The lowest values of the corrosion current density were found for the AOC samples sealed in solutions of

Table 1. Elemental surface composition of AD31 alloy after anodization and filling in nitrate solutions

Treatment conditions	Elemental composition of AOC surface, wt %								
	Al	S	O	Mg	Ca	Zn	Ni	Co	Cu
$Mg(NO_3)_2$	63.3	10.4	26.0	0.3	–	–	–	–	–
$Ca(NO_3)_2$	66.2	11.5	21.9	–	0.4	–	–	–	–
$Zn(NO_3)_2$	52.5	15.7	18.4	–	–	13.4	–	–	–
$Ni(NO_3)_2$	58.6	18.2	15.0	–	–	–	8.2	–	–
$Co(NO_3)_2$	56.6	17.3	16.0	–	–	–	–	10.1	–
$Cu(NO_3)_2$	57.7	17.1	19.1	–	–	–	–	–	6.1
$Mg(NO_3)_2$ + annealing	59.9	12.4	27.1	0.6	–	–	–	–	–
$Ca(NO_3)_2$ + annealing	63.5	12.8	23.0	–	0.7	–	–	–	–
$Zn(NO_3)_2$ + annealing	52.9	13.4	19.9	–	–	13.8	–	–	–
$Ni(NO_3)_2$ + annealing	54.2	20.6	16.4	–	–	–	8.8	–	–
$Co(NO_3)_2$ + annealing	51.9	18.7	18.8	–	–	–	–	10.6	–
$Cu(NO_3)_2$ + annealing	54.2	19.5	19.9	–	–	–	–	–	6.4

magnesium, calcium, and zinc nitrates (5.99×10^{-12}, 7.39×10^{-11}, and 1.18×10^{-10} A/cm^2, respectively).

The protective effect of sealing solutions is probably caused by hydrolysis of nitrates with the formation of poorly soluble basic salts that seal the AOC pores.

The thermal treatment of the modified AOC samples significantly changes their corrosion behaviors (Fig. 3b). In this case, the OCP values of the samples in 0.5 M NaCl solution differ by no more than 50 ± 5 mV from the unsealed sample. An exception to this is the sample sealed in the $Mg(NO_3)_2$ solution, the OCP of which shifts towards the electropositive region by 280 ± 5 mV. Analysis of the obtained polarization curves revealed that the thermal treatment of the AOC samples resulted in an increase in the corrosion current density compared to that in the untreated samples and, consequently, to a decrease in the protective ability of coatings. This effect may be caused by the cracking of the surface resulting from the heat impact. The defects facilitate the penetration of chloride ions into the AOC structure, which accelerates its corrosion failure.

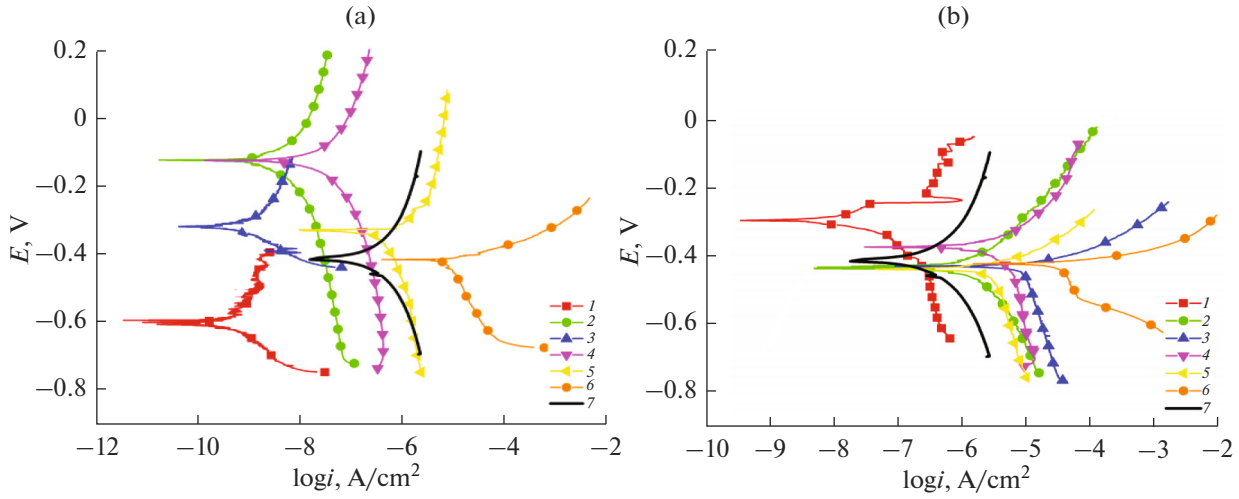

Fig. 3. Potentiodynamic polarization curves of AOC samples in 0.5 M NaCl solution: compositions of 0.2 M AOC sealing electrolyte solutions: (*1*) $Mg(NO_3)_2$, (*2*) $Ca(NO_3)_2$, (*3*) $Zn(NO_3)_2$, (*4*) $Ni(NO_3)_2$, (*5*) $Co(NO_3)_2$, (*6*) $Cu(NO_3)_2$ and (*7*) unsealed. (a) Before annealing, (b) after annealing.

Table 2. Electrochemical parameters evaluated from analysis of potentiodynamic polarization curves

Treatment conditions	a_c, V	$\|b_c\|$, V	b_a, V	a_a, V	i_{corr}, A cm^{-2}	E_{corr}, V	*EI*, %
$Mg(NO_3)_2$	−0.010	0.705	0.007	−0.519	5.99×10^{-12}	−0.250	99.9
$Ca(NO_3)_2$	−0.009	0.218	0.009	−0.032	7.39×10^{-11}	−0.697	99.903
$Zn(NO_3)_2$	−0.014	0.462	0.021	−0.118	1.18×10^{-10}	−0.476	99.846
$Ni(NO_3)_2$	−0.023	0.323	0.011	−0.026	1.43×10^{-9}	−0.744	98.128
$Co(NO_3)_2$	−0.016	0.452	0.009	−0.268	4.12×10^{-8}	−0.457	46.073
$Cu(NO_3)_2$	−0.011	0.483	0.022	−0.303	2.95×10^{-6}	−0.378	–
$Mg(NO_3)_2$ + annealing	−0.021	0.370	0.015	−0.020	1.26×10^{-10}	−0.687	99.8
$Ca(NO_3)_2$ + annealing	−0.005	0.481	0.014	−0.332	2.65×10^{-8}	−0.364	65.314
$Zn(NO_3)_2$ + annealing	−0.020	0.482	0.020	−0.191	3.76×10^{-8}	−0.462	50.785
$Ni(NO_3)_2$ + annealing	−0.005	0.481	0.014	−0.332	2.65×10^{-8}	−0.364	65.314
$Co(NO_3)_2$ + annealing	−0.021	0.511	0.017	−0.261	2.82×10^{-7}	−0.423	–
$Cu(NO_3)_2$ + annealing	−0.032	0.586	0.015	−0.350	9.29×10^{-6}	−0.377	–
Without sealing	−0.927	0.072	0.0801	−0.159	7.64×10^{-8}	−0.408	–

The highest corrosion current density (Table 2) and, consequently, the lowest corrosion resistance was observed for the samples sealed in the solutions of copper and cobalt nitrates, which showed corrosion current density i_{corr} of 2.95×10^{-6} and 4.12×10^{-8} A/cm^2, respectively. The probable reason is that the thermal treatment performed in the hot sealing solutions reinforced the hydrolyses of modifying components and the formation of their basic salts and hydroxides in the pores. Prolonged thermal exposure led to decomposing the compounds present in the pores and forming corresponding oxides. Since the particles of resultant oxides exhibit low adhesion to the AOC surface, and their dimensions are comparable with the pore sizes, they did not ensure complete blockage of the pores, which reduced the AOC corrosion resistance.

The efficiency of AOC sealing was evaluated from the values of protective effect calculated using a formula [17, 18]:

$$EI, \% = \frac{i^0_{corr} - i_{corr}}{i^0_{corr}} \times 100, \quad (1)$$

where i^0_{corr} and i_{corr} are the values of corrosion current density of the reference sample (anodized unsealed aluminum alloy) and modified sample, respectively.

As follows from Table 2, an inhibiting effect of about 99% is observed for samples that were sealed in the $Mg(NO_3)_2$, $Ca(NO_3)_2$, $Zn(NO_3)_2$, and $Ni(NO_3)_2$ solutions without consequent thermal treatment. In the case of AOC samples modified in the $Co(NO_3)_2$ and $Cu(NO_3)_2$ solutions, this effect was much lower and reached negative values. Therefore, it is useless to carry out the finish thermal treatment upon the AOC formation on aluminum alloys.

Figure 4 shows the results of impedance spectroscopy of the prepared samples as Nyquist plots. In the case of the AOC samples modified in the studied sealing solutions, two time constants could be distinguished (Fig. 4a). In the high and medium-frequency region, the first constant is a semicircle typical for electrochemical processes with a limiting stage of charge transfer. A part of the spectrum inclined to the abscissa axis at an angle of 45° is observed in the low-frequency region, which is typical for processes with a limiting diffusion stage. During the anodization and sealing, the porous AOC layer is filled with aqueous electrolytes characterized by high values of electrical conductivity [13, 14]. In this regard, the upper limit of the used frequency range may not be sufficient to record a response of the external porous AOC layer, whereas the obtained frequency dependence of the real and imaginary parts of impedance describes the corrosion process in the depth of the pores.

The thermal treatment of the samples led to changes in the character of the impedance spectra: one time constant in the form of semicircle can be distinguished on the Nyquist plots (Fig. 4b). The recorded spectra describe the resistance and the capacitive response of the barrier AOC layer, which is typical for the thermally treated coatings [16, 17].

Experimental data were fitted by the equivalent circuits, in which R_s is the resistance of the electrolyte, Ω cm^2; R_1 represents the resistance of the AOC layer, Ω cm^2; CPE_1 is the constant phase element describing the capacitive response of the AOC layer; and W is the

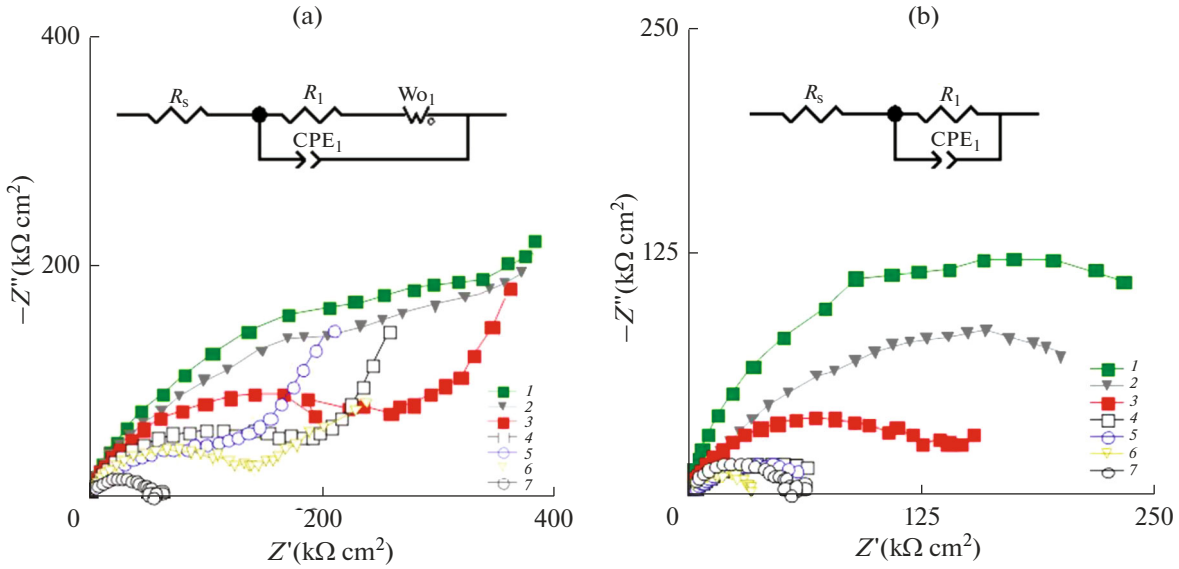

Fig. 4. Results of impedance spectroscopy depicted as a Nyquist plots: compositions of 0.2 M AOC sealing electrolyte solutions: (*1*) $Mg(NO_3)_2$, (*2*) $Ca(NO_3)_2$, (*3*) $Zn(NO_3)_2$, (*4*) $Ni(NO_3)_2$, (*5*) $Co(NO_3)_2$, (*6*) $Cu(NO_3)_2$ and (*7*) unsealed. (a) Before annealing, (b) after annealing.

Warburg impedance. The impedance of the constant phase element is fitted by two parameters: constant Y_1, Ω^{-1} cm^{-2} s^n, and mathematical factor n. The diffusional Warburg impedance includes active component W_R, Ω cm^2, and reactive component W, Ω^{-1} cm^{-2} s^n, as well as mathematical factor $n = 0.5$. Table 3 summarizes the fitting results for the equivalent circuit parameters.

Comparison of resistances of the porous AOC layer R_1 revealed that this parameter for the samples, which were not fired, exceeds that of the treated sample, which is indicative of a greater protective effect and is consistent with the data of polarization studies.

The sealing efficiency was evaluated on the basis of the values of the protective effect calculated by the formula

$$EI,\% = \frac{(R_1 + W_R) - R_1^0}{(R_1 + W_R)} \times 100, \quad (2)$$

where $(R_1 + W_R)$ and R_1^0 are the resistances of the AOC layer of the modified sample and the reference sample (anodized unsealed aluminum alloy), respectively.

Table 3. Parameters of equivalent circuits evaluated from the analysis of impedance spectroscopy data

Treatment conditions	R_1, Ω cm^2	Y_1, Ω^{-1} cm^{-2} s^n	n_1	W_R, Ω cm^2	W, Ω^{-1} cm^{-2} s^n	EI, %
$Mg(NO_3)_2$	372680	3.302×10^{-8}	0.812	380960	0.798	93.04
$Ca(NO_3)_2$	351580	1.014×10^{-8}	0.864	371380	0.531	92.74
$Zn(NO_3)_2$	212050	1.2232×10^{-8}	0.832	340960	0.407	90.51
$Ni(NO_3)_2$	158690	3.553×10^{-8}	0.822	277770	0.880	87.98
$Co(NO_3)_2$	143340	3.4438×10^{-8}	0.787	238700	0.314	86.27
$Cu(NO_3)_2$	83017	1.515×10^{-8}	0.780	213970	0.710	82.34
$Mg(NO_3)_2$ + annealing	253010	5.189×10^{-7}	0.753	–	–	79.27
$Ca(NO_3)_2$ + annealing	233010	1.4554×10^{-7}	0.690	–	–	77.45
$Zn(NO_3)_2$ + annealing	135050	2.6536×10^{-7}	0.588	–	–	61.17
$Ni(NO_3)_2$ + annealing	59457	8.1454×10^{-7}	0.641	–	–	11.8
$Co(NO_3)_2$ + annealing	51504	7.8932×10^{-7}	0.644	–	–	–
$Cu(NO_3)_2$ + annealing	32581	2.1329×10^{-7}	0.865	–	–	–
Without sealing	52436	2.2688×10^{-7}	0.871	–	–	–

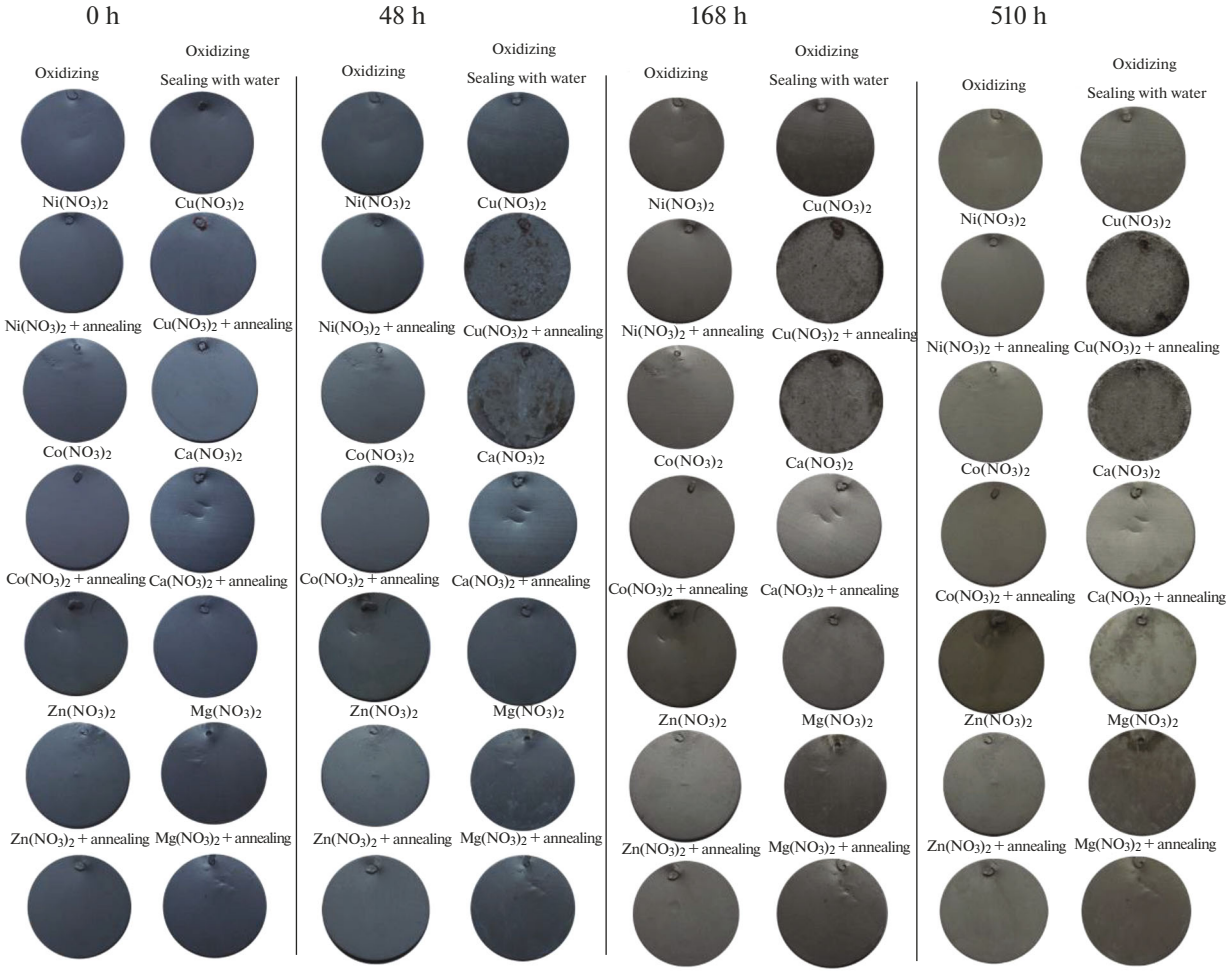

Fig. 5. Photographs of samples after tests in the salt-spay chamber.

All prepared samples were also tested in a salt-spray chamber for 510 h. Figure 5 shows photographs of the samples of AD31 aluminum alloy before and after tests. The sealing resulted in the formation of an oxide film with a characteristic matte color on the surface, and the color intensity decreases with an increase in the time of corrosion tests in the salt-spray chamber. The sealed samples, which are not thermally treated, showed high resistance to chloride-containing medium. Even after 510 h of tests, their surface structure remained almost unchanged, and no corrosion spots were found.

However, many pitting corrosion spots were found on the surface of the thermally treated samples already after 48 h of corrosion tests. After 510 h, almost the entire surface of the samples is covered with numerous white products of corrosion.

Based on the results of the conducted experiments, a mechanism of the sealing of the oxide layer formed on AD31 alloy during the sulfuric anodization was proposed (Fig. 6a).

Sulfuric acid used for anodizing is responsible for the presence of a significant amount of sulfate ions in the AOC structure, which can enter into an ion exchange reaction with Ca^{2+} ions upon the sealing of the AOCs by calcium nitrate and, thereby, close pores with poorly soluble sulfate (Fig. 6b):

$$Ca^{2+} + SO_4^{2-} \rightarrow CaSO_4. \quad (3)$$

Annealing of the AOC samples modified with calcium salts initiates the formation of "dead gypsum."

Divalent metal nitrates and sulfates formed by a strong acid and a weak base are sensitive to hydrolysis resulting in the formation of corresponding cation $MeOH^+$:

$$Me^{2+} + H_2O \Leftrightarrow MeOH^+ + H^+. \quad (4)$$

Since the value of the second constant of electrolytic dissociation of copper hydroxide is $K_d = 10^{-7}$, which is two to three orders of magnitude less than for hydroxides of other metals, copper salts are sensitive to hydrolysis to a greater extent. The heating of sealing

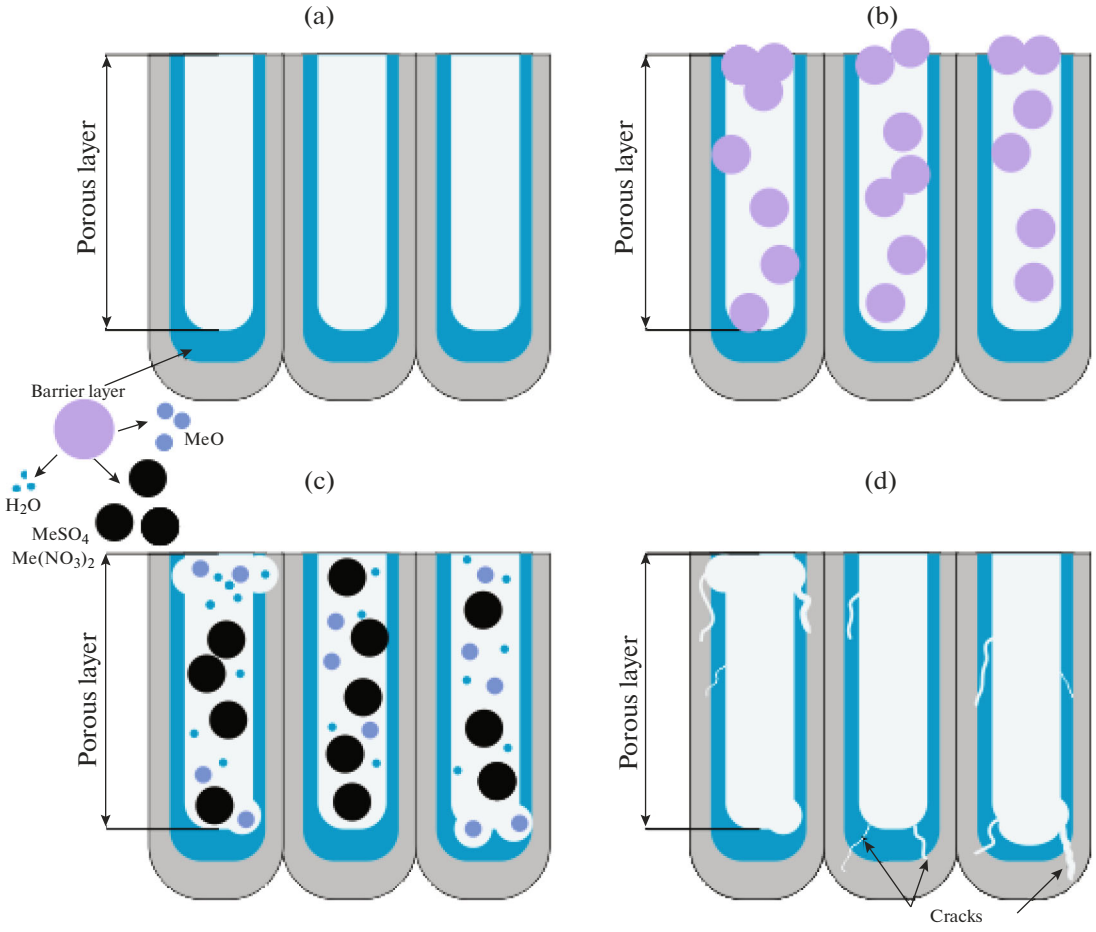

Fig. 6. Mechanism of AOC sealing.

solutions leads to the intensification of the hydrolysis processes. Also, it promotes the decomposition of the poorly soluble bases and base salts with the formation of corresponding oxides and neutral salts.

$$Me(OH)_2 \xrightarrow{t} MeO + H_2O, \quad (5)$$

$$(MeOH)_2SO_4 \rightarrow MeSO_4 + MeO + H_2O, \quad (6)$$

$$2MeOHNO_3 \rightarrow Me(NO_3)_2 + MeO + H_2O. \quad (7)$$

The resulting salts of copper, zinc, nickel, and cobalt are readily soluble in water, and their oxides are characterized by low adsorption capacity toward aluminum oxide. The resulting compounds of these metals can pass from the pores into the solution along with the formation of defects in the boehmite structure of the oxide layer. In this case, the pore remains open, facilitating the diffusion of aggressive chloride-ions to the aluminum matrix (Fig. 6c).

When using magnesium nitrate solution for sealing, poorly soluble magnesium hydroxides and oxides are formed in the modified AOC samples with a sufficiently high adsorption capacity towards the porous layer of aluminum oxide. This phenomenon results in denser AOCs, which provide reliable protection of the aluminum substrate from the aggressive action of surrounding media.

Subsequent thermal treatment of the sealed AOC samples contributes to decomposing the salts in the pores and forming additional amounts of modifying metal oxides under study. However, due to a significant difference between the coefficients of volumetric expansion of the aluminum matrix and the formed coating, the thermal treatment leads to cracking of AOCs and emerging local defects in the AOC structure (Fig. 6d), which, in general, significantly reduces the protective properties of the surface.

CONCLUSIONS

1. SEM data revealed that the sealing of anodized AD31 aluminum alloy resulted in the formation of coatings with numerous microinclusions. Subsequent

thermal treatment deepened the total heterogeneity of the coating surface, gave rise to local defects, and led to an increase in the number of microcracks in the coating structure, which was attributed to the significant difference between the thermal expansion of the aluminum matrix and oxide layer.

2. Results of EDX analysis provided evidence that the main components of the formed coatings were aluminum, oxygen, and sulfur. The content of modifying metals in the AOC structure ranged from 0.30 to 13.40 wt %, depending on the sealing electrolyte composition. The thermal treatment at 300°C led to an increase in the modifying agent content in the coating structure by 0.30–0.50 wt %.

3. Polarization experiments showed an inhibiting effect of about 99% for AOC samples sealed in the $Mg(NO_3)_2$, $Ca(NO_3)_2$, $Zn(NO_3)_2$, and $Ni(NO_3)_2$ solutions. Subsequent thermal treatment had a negative effect on corrosion resistance of the samples (the protective action was not more than 65%), which was caused by the cracking of the AOC samples and the formation of local defects in their structure.

4. Tests in a salt-spray chamber for 510 h revealed no corrosion spots in the AOC samples modified by calcium, magnesium cations, as well as the cations of some transition 3*d* metals, but not subsequently thermally treated. In contrast, as early as 48 h after the tests, the corrosion pits were fixed on the surface of the modified AOC samples, which were thermally treated at 300°C for 30 min. After 510 h, numerous white corrosion products covered almost the entire surface of the sample.

REFERENCES

1. Evertsson, J., Bertram, F., Rullik, L., Harlow, G., and Lundgren, E., *J. Electroanal. Chem.,* 2017, vol. 799, pp. 556–562.
2. Stojadinović, S., Vasilić, R., Kasalica, B., Belča, I., and Zeković, L., in *Modern Aspects of Electrochemistry,* vol. 57: *Electrodeposition and Surface Finishing,* Djokic, S., Ed., New York: Springer, 2014. https://doi.org/10.1007/978-1-4939-0289-7_5.
3. Zhang, F., Nilsson, J., and Pan, J., *J. Electrochem. Soc.,* 2016, vol. 163, no. 9, pp. C609–C618.
4. Jeong, C., Lee, J., Sheppard, K., and Choi, C., *Langmuir,* 2015, vol. 31, pp. 11040–11050.
5. Hao, L. and Cheng, R., *Met. Finish.,* 2000, vol. 98, pp. 8–18.
6. Ofoegbu, S.U., Fernandes, F.A.O., and Pereira, A.B., *Coatings,* 2020, vol. 10, p. 226.
7. Chahboun, N., Rocca, E., Veys-Renaux, D., Augros, M., Boutoba, M., and Caldeira, N., *J. Electrochem. Soc.,* 2016, vol. 163, no. 3, pp. C69–C75.
8. Yu, X. and Cao, C., *Thin Solid Films,* 2003, vol. 423, pp. 252–256.
9. Osipenko, M.A., Kharitonov, D.S., Makarova, I.V., Wrzesińska, A., and Kurilo, I.I., *Prot. Met. Phys. Chem. Surf.,* 2020, vol. 56, no. 5, pp. 990–997.
10. Kharitonov, D.S., et al., *J. Electrochem. Soc.,* 2018, vol. 165, no. 3, pp. 116–126.
11. Kharitonov, D.S., et al., *Corros. Sci.,* 2020, vol. 171, p. 108658.
12. Kharitonov, D.S., et al., *Prot. Met. Phys. Chem. Surf.,* 2018, vol. 54, pp. 291–300; Kharitonov, D.S., et al., *Prot. Met. Phys. Chem. Surf.,* 2020, vol. 56, pp. 113–124.
13. Liu, W., Zuo, Y., Chen, S., Zhao, X., and Zhao, J., *Surf. Coat. Technol.,* 2009, vol. 203, no. 9, pp. 1244–1251.
14. Balaraju, J.N., Srinivasan, A., Yoganandan, G., Grips, V.K.W., and Rajam, K.S., *Corros. Sci.,* 2011, vol. 53, no. 12, pp. 4084–4092.
15. Runge, J.M., in *The Metallurgy of Anodizing Aluminum,* Cham: Springer, 2018. https://doi.org/10.1007/978-3-319-72177-4_3.
16. Donahue, C.J. and Exline, J.A., *J. Chem. Educ.,* 2014, vol. 91, pp. 711–715.
17. Chang, J., Lin, C., Liao, C., and Chen, C., *J. Electrochem. Soc.,* 2004, vol. 151, p. B188.
18. Amin, M.A., Ei-Rehim, S.S.A., El-Sherbini, E.E.F., Hazzazi, O.A., and Abbas, M.N., *Corros. Sci.,* 2009, vol. 51, no. 3, pp. 658–667.

Translated by E. Khozina